Anisotropic thermal expansion of layered MoO_3 crystals

Hiroshi Negishi,[1,*] Saiko Negishi,[1] Yoshihiro Kuroiwa,[2] Nobufumi Sato,[2] and Shinobu Aoyagi[3]
[1]*Graduate School of Advanced Sciences of Matter, Hiroshima University, 1-3-1 Kagamiyama, Higashi-Hiroshima 739-8530, Japan*
[2]*Department of Physics, Faculty of Science, Okayama University, 3-1-1 Tsushima, Okayama 700-8530, Japan*
[3]*Japan Synchrotron Radiation Research Institute (JASRI), 1-1-1 Kouto, Mikazuki, Sayo, Hyogo 679-5198, Japan*
(Received 4 October 2003; revised manuscript received 19 November 2003; published 24 February 2004; publisher error corrected 2 March 2004)

A structural study of orthorhombic molybdenum trioxide MoO_3 with a layered structure has been performed using synchrotron-radiation powder diffraction from 110 to 1000 K. MoO_3 exhibits an anisotropic thermal expansion. With increasing temperature, the lattice expands remarkably along the *a* axis of the stacking direction, while it expands a little along the *c* axis but contracts slightly along the *b* axis. Based on the quasiharmonic approximation, the temperature variations in the lattice constants and thermal expansion coefficient are analyzed and they are reproduced quantitatively using three stretching mode frequencies for Mo—O bonds, 1000, 820, and 670 cm^{-1}, as well as two low frequencies, 250 and 100 cm^{-1}. The large thermal expansion along the *a* axis is attributed to the coexistence of high frequency vibration due to the covalent Mo—O bond and high compressibility due to the van der Waals gaps in MoO_3.

DOI: 10.1103/PhysRevB.69.064111 PACS number(s): 61.10.Nz, 65.40.De, 61.66.Fn

I. INTRODUCTION

Molybdenum trioxide MoO_3 is well known as a layered material having a variety of potentials in many fields, such as catalyses,[1] photoluminescence,[2] photochromisms,[3] batteries,[4] and a starting material of charge-density-wave (CDW) materials of Mo_4O_{11} and $K_{0.30}MoO_3$.[5–7] Furthermore, nanobelts and nanotubes of MoO_3 have been obtained recently, and they are expected to extend their capabilities to various applications.[8,9]

Most recently, the electron density (ED) distribution of MoO_3 has been obtained at 300 K by analyzing the precise powder diffraction data using the maximum entropy method (MEM)/Rietveld method.[10] MoO_3 has an orthorhombic unit cell with the space group of *Pnma* (*Pbnm*, in which the orientation is nonstandard, was used by Kihlborg[11]) and it contains four formula units of MoO_3 in the unit cell. There are one Mo atom and three nonequivalent O atoms (referred to as O1, O2, and O3 in Fig. 1). The crystal is built up by the stacking of the distorted MoO_5 pyramid layers along the *a* axis, as shown in Fig. 1. The MEM ED study confirms that the Mo—O3 bond with the shortest bond length 1.635 Å along the *a* axis is strongly covalent, and the covalent Mo—O2 bonds with 1.744 Å (Mo—O2a) and 2.241 Å (Mo—O2b) along the *c* axis and the Mo—O1 bonds with 1.956 Å (Mo—O1a and Mo—O1c) along the *b* axis form a two-dimensional (2D) bonding network. The value of the minimum ED of the Mo—O3 bond is $1.99\,e\text{Å}^{-3}$, much larger than others of 1.78, 0.79, and $0.63\,e\text{Å}^{-3}$ for the Mo—O2a, Mo—O1a (1c), and Mo—O2b bonds, respectively. Moreover, the ionic states of Mo and O1, O2, and O3 atoms are evaluated to be in $+3.0(1)$, $-1.6(1)$, $-0.7(1)$, and $-0.8(1)$, respectively, in good agreement with the values predicted by the recent calculations,[12] but much different from the values for the fully ionic states, $+6$ and -2 for Mo and O, respectively, used frequently to discuss a bond strength and ionic state from interatomic distance between Mo and O atoms.[13]

On the other hand, CDW molybdenum oxides, one-dimensional (1D) conductor $K_{0.30}MoO_3$ (Ref. 14) and 2D conductor η-Mo_4O_{11} (Ref. 15), show noticeable CDW-induced changes in the lattice parameters. However, to our knowledge, there is no report about the temperature dependence of lattice parameters in MoO_3, except for the pioneering work by Kierkegaard in 1964 which gives simply the linear thermal expansion coefficients averaged over 25–500 °C.[16] Here we report the structural studies of MoO_3. Temperature variations of the lattice constants confirm an anisotropic thermal expansion. Such a behavior is analyzed based on the phonon modes, using anisotropic positive and negative Grünneisen parameters. They are discussed in terms of the bond characteristics in MoO_3.

II. EXPERIMENT

Single crystals of MoO_3 were grown by a chemical vapor transport technique.[17] High-resolution powder-diffraction experiments were performed using synchrotron radiation with a wavelength of $\lambda = 0.65338$ Å and a large Debye-Scherrer camera with an imaging plate as a detector installed at BL02B2 in SPring-8.[18,19] Data were collected at 110 and 300 K to obtain the crystal structure parameters for a pulverized sample by the Rietveld refinements. Those for another pulverized sample were collected from 300 to 1000 K in steps of 100 K to obtain the lattice constants *a*, *b*, and *c*. The sublimation and recrystallization of the pulverized sample occurred at 1000 K, which made it difficult to determine the structural parameters above 1000 K.

III. RESULTS AND DISCUSSION

The structure of MoO_3 has been determined using the Rietveld method with a space group of *Pnma*. The refinement was done for the data in $2\theta < 72°$ ($d = 0.584$ Å). At first, we shall concern ourselves with the structures at 110 and 300 K. The powder diffraction pattern observed at 110 K was well reproduced by the refined diffraction pattern, as

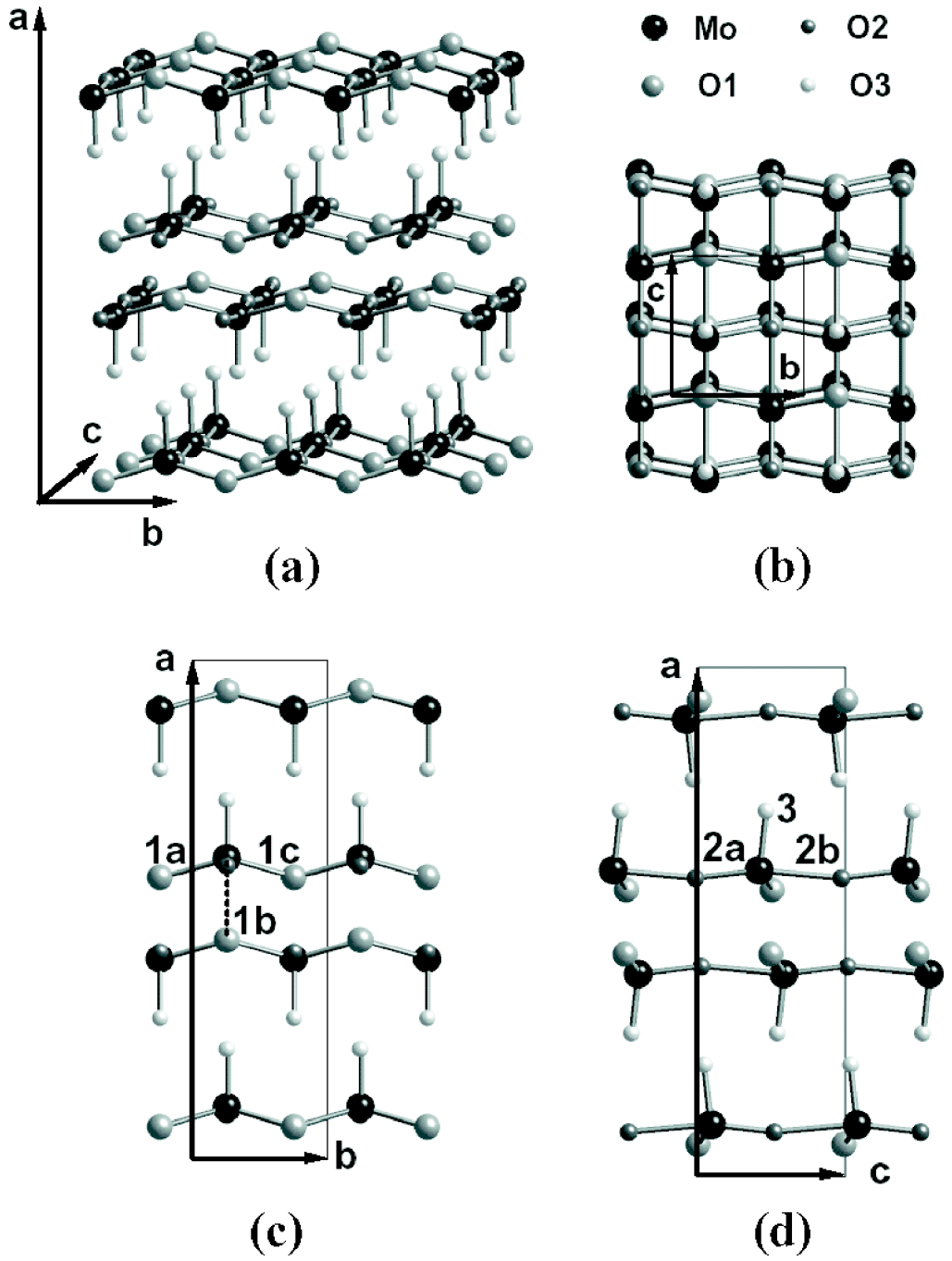

FIG. 1. (a) Crystal structure of MoO_3 in perspective. Projections on (b) the *bc* plane, (c) the *ab* plane, and (d) the *ca* plane, where the *a*, *b*, and *c* axes are taken in the crystal symmetry of *Pnma*, instead of *Pnmb* used by Kihlborg (Ref. 11). Crystallographically nonequivalent O atoms are distinguished by O1, O2, and O3. The distorted MoO_5 pyramids form two-dimensional layers and they are stacked along the *a* axis. The values of the interatomic distance between Mo and surrounding O atoms denoted by 1a, 1b, 1c, 2a, 2b, and 3 are listed in Table II.

shown in Fig. 2. The reliability factors are excellent as $R_{WP}=5.04\%$, $R_I=2.96\%$, and $R_F=1.84\%$ for 110 K, and $R_{WP}=4.47\%$, $R_I=2.80\%$, and $R_F=1.48\%$ for 300 K. The obtained structural parameters are listed in Table I. The ED map obtained from the MEM/Rietveld analysis for the powder data at 300 K has been already reported.[10] The lattice parameter *a* expands remarkably by 0.10 Å, and *c* expands slightly by 0.0065 Å, while *b* oppositely shrinks slightly by -0.0014 Å from 110 to 300 K. Bond lengths *d* between Mo and O*i* atoms ($i=1,2,3$) are evaluated from the atomic positions in Table I; the results are listed in Table II. The shortest bond length between the Mo—O3 atoms decreases from 1.6820 Å at 110 K to 1.6352 Å at 300 K by 0.0468 Å, but other bond lengths increase with increasing temperature, at most by 0.0054 Å, except for 0.014 Å for the bondless Mo—O1b with the low ED of 0.37 $e\text{Å}^{-3}$ (Ref. 10). This

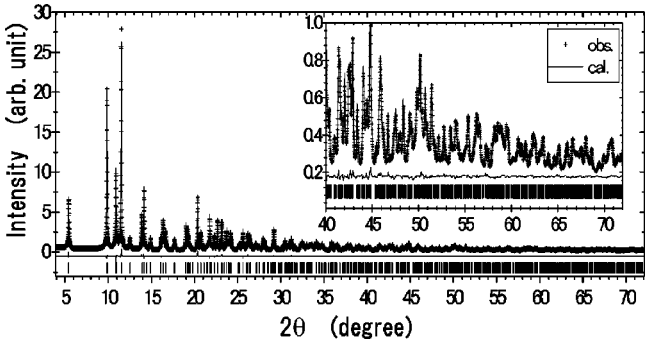

FIG. 2. Observed powder diffraction pattern and fitting result of the Rietveld refinement of MoO_3 at 110 K; the inset is magnification of the high-angle region.

shortening of the Mo—O3 length, at first glance, seems to be inconsistent with the remarkable increase of a ($\Delta a = 0.10$ Å). The increase of the Mo—O1b distance, 0.014 Å, is not enough to explain the variation in a. Here, we should recall the existence of the van der Waals gaps perpendicular to the a axis. The lattice parameter a is given roughly by the sum of the Mo—O3 bond length, the Mo—O1b distance, and the van der Waals gap distance d_{vdW} between O3 layers. From the atomic position of O3 atom (Table I), d_{vdW} is evaluated to be 0.744 Å at 110 K and 0.865 Å at 300 K, indicating an increase of 0.121 Å, which is much larger than the variations of the Mo—O3 bond length and Mo—O1b distance. Thus, the observed increase of a is mainly due to the expansion of the van der Waals gap with temperature.

The thermal parameter B, which is obtained assuming isotropic thermal motions of atoms, increases from O1, O2, and Mo to O3 atoms in order. Atomic mean square thermal displacement $(\langle u^2 \rangle)^{1/2}$, hereafter referred as u in short, is evaluated using the relation $B = 8\pi^2 \langle u^2 \rangle$; for O1, O2, Mo, and O3 atoms, respectively, $u = 0.02(2)$, 0.045(6), 0.0610(0), and 0.072(4) Å at 110 K, and 0.034(8), 0.063(4), 0.0646(2), and 0.083(4) Å at 300 K. The temperature variation in u is larger for O1 and O2 atoms than Mo and O3 atoms. From the anisotropic thermal parameters obtained from the detailed refinements at 300 K,[10] moreover, the thermal motions of O1 and O3 atoms are nearly isotropic [$u = 0.03(2)$ and 0.084(6) Å, respectively], but those of O2 and Mo atoms are weakly and seriously anisotropic, respectively. For Mo atom, especially, thermal displacements are large along the a and c axes [$u = 0.0775(6)$ and 0.0721(6) Å, respectively] comparable to that of O3 atom, but small along the b axis [$u = 0.039(1)$ Å] nearly equal to that of the O1 atom. Thus, Mo atom moves mainly in the ac plane. Such variations in the thermal displacements can be understood in terms of bond nature of MoO_3. As confirmed by the MEM ED study,[10] the O1c—Mo—O1a bond along the b axis is symmetrical and strong with the minimum ED of $0.79\, e\text{Å}^{-3}$, while the Mo—O3 and O2a—Mo—O2b bonds are asymmetric along the a and c axes, respectively. The Mo—O3 bond is remarkably strong covalent but the O3—O3 bond is distinguishably weak by the vdW force, and Mo—O2a is strongly covalent but Mo—O2b is rather weakly covalent. The Mo—O3 bond is very rigid and moves thermally easily along the a axis but hard in the bc plane due to the 2D bonding network, leading that the values of u (and B) are large for O3 and Mo atoms, but small for O1 and O2 atoms at 110 K. Since at 300 K the stretching modes for the Mo—O bonds are rarely excited and the bending phonon modes with low frequencies are excited, the O2—Mo—O3

TABLE II. Interatomic distance between Mo and O atoms in MoO_3 at 110 and 300 K, and its difference Δd ($= d_{300\mathrm{K}} - d_{110\mathrm{K}}$) evaluated from the values in Table I. For the notation of the O atom surrounding Mo atom, see Fig. 1.

Mo—O	$d_{110\mathrm{K}}$ (Å)	$d_{300\mathrm{K}}$ (Å)	Δd (Å)
O3	1.682(1)	1.635(1)	−0.047(2)
O2a	1.738(1)	1.744(1)	0.005(2)
O1a	1.956(1)	1.956(1)	0.001(2)
O1c	1.956(1)	1.956(1)	0.001(2)
O2b	2.240(1)	2.241(1)	0.001(2)
O1b	2.291(1)	2.305(1)	0.014(2)

TABLE I. Lattice constnats a, b, and c, atomic position x, y, and z, and thermal factor B of Mo and O atoms (O1, O2, O3) in orthorhombic MoO_3 at 110 and 300 K. Space group: *Pnma*.

	a (Å)	b (Å)	c (Å)		
110 K	13.7644(1)	3.69894(3)	3.95640(3)		
300 K	13.8649(1)	3.69756(2)	3.96290(3)		
	Atom	x	y	z	B (Å^2)
110 K	Mo	0.10163(3)	0.25	0.08461(8)	0.2943(3)
	O1	0.4368(1)	0.25	0.4957(4)	0.02(4)
	O2	0.0867(1)	0.25	0.5209(4)	0.16(4)
	O3	0.2230(1)	0.25	0.0352(5)	0.41(5)
300 K	Mo	0.10163(3)	0.25	0.08461(8)	0.329(2)
	O1	0.4370(1)	0.25	0.4963(5)	0.09(4)
	O2	0.0869(1)	0.25	0.5216(4)	0.31(4)
	O3	0.2188(1)	0.25	0.0376(5)	0.55(5)

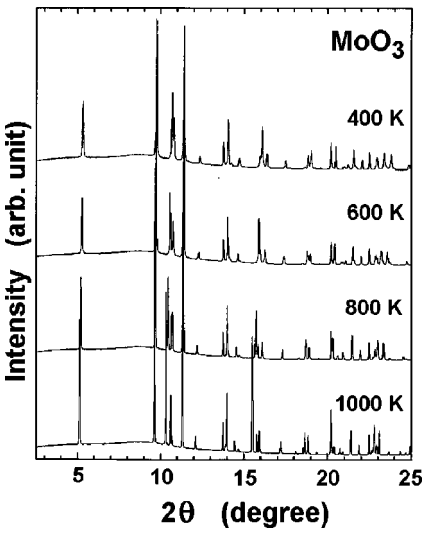

FIG. 3. Powder diffraction patterns of MoO_3 at 400, 600, 800, and 1000 K.

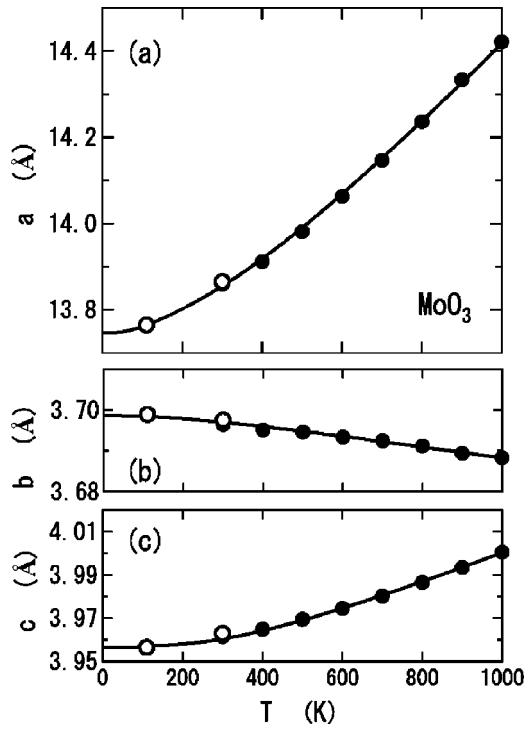

FIG. 4. Temperature variation in the lattice constants (a) *a*, (b) *b*, and (c) *c* of MoO_3. The solid line is the calculated result by Eq. (8) based on the quasiharmonic approximation using five phonon frequencies. The values employed are listed in Table III (see the text for more details).

block rotates, accompanying the displacement of O2 atom in the *ac* plane and the displacement of O1 atom in the *ab* plane, leading to increases of *u* of O1 and O2 atoms with temperature, as well as an expansion of d_{vdW} on an increase of the effective van der Waals radius of the O3 atom. The shortening of the Mo—O3 bond length with temperature evaluated above does not mean a shortening of the real Mo—O3 bond length but means a shift of the averaged thermal position of the O3 atom to the averaged position of Mo atom along the *a* axis, which occurs as a result of the rotational thermal motions of the O2—Mo—O3 block with an almost unchanged Mo—O3 length. Furthermore, the decrease of *b* in spite of the increase of the Mo—O1 bond length is attributable to the decrease of the angle of the O1—Mo—O1 bond from 142.09° at 110 K to 141.82° at 300 K.

Next, we shall show temperature variation in the structure above 300 K. Figure 3 shows the powder diffraction patterns of another MoO_3 sample observed at different temperatures. It can be seen that some peaks shift drastically to the lower angle side, but other peaks remain almost unchanged. The obtained lattice parameters are plotted in Fig. 4 (solid circles), together with those for the sample at 110 and 300 K mentioned above (open circles). The difference in the lattice constants at 300 K for the samples is so small, at most 0.04%, that it can be neglected in the following discussion. With increasing temperature, the lattice parameter *a* expands remarkably and *c* expands slightly up to 1000 K, while *b* decreases oppositely. Such behaviors are consistent with the changes between the lattice parameters at 110 and 300 K. Thus, MoO_3 shows a strongly anisotropic thermal expansion. Figure 5 show the temperature dependence of the unit cell volume $V\ (=abc)$ and the bulk thermal expansion coefficient $\alpha_V\ [=(1/V)(dV/dT)]$, as well as the linear expansion coefficient α_x, which is given by $\alpha_x=(1/x)(dx/dT)$ for $x=a$, *b*, and *c*. The values of α_V change from $\alpha_V=4.2\times10^{-5}\ \mathrm{K}^{-1}$ at 300 K to $7.5\times10^{-5}\ \mathrm{K}^{-1}$ at 1000 K, indicating some contributions of phonon modes with high frequencies to the thermal expansion. The linear expansion coefficient α_x is remarkably anisotropic, as $\alpha_a \gg \alpha_c > 0 > \alpha_b$. Therefore, the main component of α_V is that of the *a* axis ($\alpha_V \cong \alpha_a+\alpha_b+\alpha_c \sim \alpha_a$), along which the layers are stacked by the van der Waals force. Such an anisotropy in α_x was also reported by Kierkegaard;[16] $\alpha_a=18(2)\times10^{-5}\ \mathrm{K}^{-1}$, $\alpha_b=0\times10^{-5}\ \mathrm{K}^{-1}$, and $\alpha_c=0.9(1)\times10^{-5}\ \mathrm{K}^{-1}$. Quantitatively, however, the reported value of α_a is significantly larger by 3–4 times than the present result of $\alpha_a=(4-6)\times10^{-5}\ \mathrm{K}^{-1}$ (Fig. 5).

Here, we shall compare the thermal expansion of MoO_3 with those of $K_{0.30}MoO_3$ and η-Mo_4O_{11}. In $K_{0.30}MoO_3$,[14] the thermal expansion coefficient is $7.5\times10^{-5}\ \mathrm{K}^{-1}$ around 300 K, about two times that of $4.2\times10^{-5}\ \mathrm{K}^{-1}$ in MoO_3. This material shows less expansion along the *b* axis, but a large expansion both along the [102] and $[\bar{2}01]$ directions in the (010) plane, indicating that the MoO_6 octahedra are connected strongly along the *b* axis, but rather weakly along the [102] direction to form the slabs, and they are stacked along the $[\bar{2}01]$ direction via K atoms. The linear expansion coefficient along the $[\bar{2}01]$ direction in $K_{0.30}MoO_3$ is large and comparable to that by van der Waals gaps along the *a* axis in MoO_3. In η-Mo_4O_{11},[15] on the other hand, the value of $\alpha_V=0.85\times10^{-5}\ \mathrm{K}^{-1}$ at 300 K is much smaller than that in MoO_3, indicating that the 2D covalent bonding network with the edge-sharing structure of the MoO_6 octahedra are

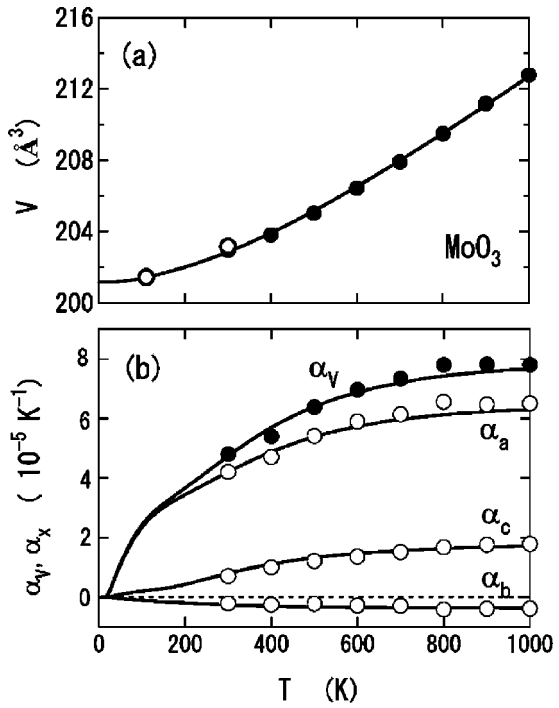

FIG. 5. Temperature variation in (a) the unit cell volume V and (b) the thermal expansion coefficient α_V of MoO_3, together with the linear expansion coefficients α_a, α_b, and α_c. Solid lines are the calculated results based on the quasiharmonic approximation using five phonon frequencies.

bridged strongly by MoO_4 tetrahedra along the stacking direction. In both materials, due to a CDW-induced lattice instability, the remarkable variation in lattice constants occurs below the transition temperatures, as reported. Thus, we can control the thermal expansion by inserting the guest atoms into the van der Waals gaps of MoO_3 to keep a large expansion along the stacking direction, or by a structural modification induced from the poor oxygen stoichiometry to be more rigid along the stacking direction.

Now we shall discuss the thermal expansion of MoO_3 based on the lattice dynamics. Within a quasiharmonic approximation,[20] the free energy F is given by the sum of a static elastic energy Φ_{el} and the vibrational free energy F_{vib}, $F \cong \Phi_{el} + F_{vib}$, and the equation of state is derived by $p = -(\partial F/\partial V)_T$. For phonon system with vibrational frequency ω_s, F_{vib} is given by

$$F_{vib} = (1/2)\sum_s \hbar\omega_s + k_B T \sum_s \ln[1 - \exp(-\hbar\omega_s/k_B T)]. \tag{1}$$

Expanding Φ_{el} and F_{vib} by $(V - V_0)$ around the equilibrium volume V_0,

$$\Phi_{el} \cong \Phi_{el}(V_0) + \frac{1}{2}(\partial^2\Phi_{el}/\partial V^2)_{V_0}(V - V_0)^2,$$

$$F_{vib} \cong F_{vib}(V_0) + (\partial F_{vib}/\partial V)_{V_0}(V - V_0), \tag{2}$$

the equation of the state can be written as

$$pV_0 = -[(V - V_0)/\kappa_0] + \sum_s \gamma_s \hbar\omega_s \times \{1/2 + 1/[\exp(\hbar\omega_s/k_B T) - 1]\}, \tag{3}$$

with the compressibility $\kappa_0 = [V_0(\partial^2\Phi_{el}/\partial V^2)_{V_0}]^{-1} = -(\partial V/\partial P)_{V_0}/V_0$ and the Grünneisen constant $\gamma_s = \partial \ln \omega_s / \partial \ln V$ for each phonon mode with ω_s. Thus, by replacing $p = 0$, we obtain thermal expansion $\varepsilon \equiv (V - V_0)/V_0$,

$$\varepsilon = (\kappa_0/V_0)\sum_s \gamma_s \hbar\omega_s \{1/2 + 1/[\exp(\hbar\omega_s/k_B T) - 1]\}. \tag{4}$$

Furthermore, a linear thermal expansion ε_x for $x = a$, b, and c in an orthorhombic system, defined by $\varepsilon_x \equiv (x - x_0)/x_0$, is given by

$$\varepsilon_x = (\kappa_{0x}/V_0)\sum_s \gamma_{sx} \hbar\omega_s \{1/2 + 1/[\exp(\hbar\omega_s/k_B T) - 1]\}, \tag{5}$$

with a linear compressibility $\kappa_{0x} = -(\partial x/\partial p)_{x_0}/x_0$, a lattice constant x_0 at $T = 0$ with no quantum effect of zero-point vibrations, and an anisotropic linear Grünneisen constant along the x axis, $\gamma_{sx} = -(\partial \ln \omega_s/\partial x)_{x_0}$. Then the lattice constant is given by

$$x = x_0 + \kappa_{0x}(x_0/V_0)\sum_s \gamma_{sx} \hbar\omega_s \times \{1/2 + 1/[\exp(\hbar\omega_s/k_B T) - 1]\}. \tag{6}$$

Here, it should be noted that the lattice constant at $T = 0$, which is referred as $x(0)$, is larger than x_0 by a quantum effect of zero-point vibrations, $\kappa_{0x}(x_0/V_0)\Sigma_s \gamma_{sx} \hbar\omega_s/2$. Similarly, $V(0)$ at $T = 0$ with quantum effect of zero-point vibrations is larger than V_0 by $\kappa_0 \Sigma_s \gamma_s \hbar\omega_s/2$. Bulk thermal expansion parameters are related to linear ones, $\kappa_0\gamma_s = -(\partial \ln \omega_s/\partial p) = \Sigma_s - (\partial \ln \omega_s/\partial \ln x)(\partial \ln x/\partial p)$, and

$$\kappa_0\gamma_s = \sum_x \kappa_{0x}\gamma_{sx} = \kappa_{0a}\gamma_{sa} + \kappa_{0b}\gamma_{sb} + \kappa_{0c}\gamma_{sc}. \tag{7}$$

Thus, we can evaluate temperature variation of lattice constants and volume, using values a_0, b_0, c_0, and $\kappa_{0x}\gamma_{sx}$ for each phonon mode with frequency ω_s, as parameters.

According to Py *et al.*,[21] orthorhombic MoO_3 has 48 vibrational modes, the representation of which is given by $\Gamma_{\text{crystal}} = 8A_g + 8B_{1g} + 4B_{2g} + 4B_{3g} + 4A_u + 4B_{1u} + 8B_{2u} + 8B_{3u}$. Phonon frequencies in MoO_3 are determined from many Raman and infrared spectroscopic studies,[21–23] which are interpreted in terms of the valence-force-field model using stretching and bending force constants.[21] Among them, there are 12 stretching modes and they are divided into three groups with high frequencies of about 1000, 820, and 670 cm^{-1} consisting of four nearly degenerate modes which are assigned to the stretching modes of Mo—O3 along the a axis, Mo—O2 along the c axis, Mo—O1 along the b axis,

TABLE III. Values used for the reproduction of the experimental lattice constants *a*, *b*, and *c* in Fig. 4 using Eq. (8) and the unit cell volume *V* in Fig. 5. Lattice parameter x_0 and $n_i\kappa_{0x}\gamma_{ix}$ for the *i*th phonon mode frequency $\hbar\omega_i$ (in units of cm^{-1}) along the *x* axis ($x=a$, *b*, and *c*), and the unit cell volume V_0 and $n_i\kappa_0\gamma_i$ (in units of 10^{-3} GPa^{-1}).

	Axis	*a*	*b*	*c*	Bulk
	x_0 (Å)	13.350 (4)	3.703(1)	3.918(1)	193.69(9) Å^3
i	$\hbar\omega_i$	$n_i\kappa_{0a}\gamma_{ia}$	$n_i\kappa_{0b}\gamma_{ib}$	$n_i\kappa_{0c}\gamma_{ic}$	$n_i\kappa_0\gamma_i$
1	1000	480(20)	0	0	484(20)
2	820	0	0	222(10)	230(10)
3	670	0	−26.7(27)	0	−28(3)
4	250	280(10)	−13.3(13)	22(2)	290(11)
5	100	280(10)	−13.3(13)	22(2)	290(11)

respectively. Corresponding stretching force constants are 791.5, 466, and 177 N/m, indicating that the shorter bond has the stronger force constant. The other 36 modes, including three acoustic modes, are below 500 cm^{-1}.

We have evaluated the values of lattice constants *a*, *b*, *c*, and *V*. For simplicity, neglecting the difference in frequency of less than 10 cm^{-1}, we may reduce the number of parameters used. For the *i*th phonon frequency ω_i with the degenerate number n_i, Eq. (6) is rewritten as

$$x = x_0 + \kappa_{0x}(x_0/V_0)\sum_i n_i\gamma_{ix}\hbar\omega_i \times\{1/2 + 1/[\exp(\hbar\omega_i/k_BT)-1]\}. \quad (8)$$

At first, we have employed only stretching modes. We take three phonon frequencies $\omega_i=1000$, 820, and 670 cm^{-1} for $i=1$, 2, and 3, and they are degenerate with $n_i=4$. Furthermore, we assume that these stretching modes contribute effectively on the thermal expansion only along the stretching directions, and take only γ_{1a}, γ_{3b}, γ_{2c} to be nonzero, and the others zero ($\gamma_{2a}=\gamma_{3a}=0$; $\gamma_{1b}=\gamma_{2b}=0$; $\gamma_{1c}=\gamma_{3c}=0$). In that case, the experimental results are reproduced well at temperatures higher than 400 K, and poor below 300 K, and not shown here. This is due to the disregard for the low frequency phonon modes. Next, we consider two additional phonon modes with low frequencies of 100 and 250 cm^{-1} ($n_i=18$) for $i=4$ and 5, to be representative of many modes with lower frequencies below 500 cm^{-1}. These modifications lead to the excellent reproduction of experimental data over whole temperature range measured, as indicated by the solid lines in Figs. 4 and 5, where the parameters used are only three along each direction with assuming $\gamma_{4x}=\gamma_{5x}$ for simplicity (Table III). The evaluated values of $x(0)$, $V(0)$, linear and bulk Grünneisen constants are also listed in Table IV.

The magnitude of the contribution of the *i*th phonon mode on the lattice parameter *x* is expressed by the parameter $n_i\kappa_{0a}\gamma_{ia}$. Along the *a* axis, $4\kappa_{0a}\gamma_{1a}$, $18\kappa_{0a}\gamma_{4a}$, and $18\kappa_{0a}\gamma_{5a}$ are 0.480, 0.280, and 0.280 GPa^{-1}, respectively, and its ratio is 1.74:1:1. Along the *b* axis, on the other hand, $4\kappa_{0b}\gamma_{3b}$, $18\kappa_{0b}\gamma_{4b}$, and $18\kappa_{0b}\gamma_{5b}$ are negative to be −26.7, −13.3, and -13.3×10^{-3} GPa^{-1}, respectively, corresponding to the construction of *b* with increasing temperature. The ratio is $4\kappa_{0b}\gamma_{3b}:18\kappa_{0b}\gamma_{4b}:18\kappa_{0b}\gamma_{5b}=2:1:1$. Those along the *c* axis, $4\kappa_{0c}\gamma_{2c}$, $18\kappa_{0c}\gamma_{4c}$, and $18\kappa_{0c}\gamma_{5c}$, are 222, 22, and 22×10^{-3} GPa^{-1}, respectively, and the ratio is $4\kappa_{0c}\gamma_{2c}:18\kappa_{0c}\gamma_{4c}:18\kappa_{0c}\gamma_{5c}=10:1:1$. Thus the contribution from three stretching modes is about two times larger than those from the two lower phonon modes along the *a* and *b* axes, and ten times along the *c* axis. Bulk parameters are also obtained using Eq. (7); $n_i\kappa_0\gamma_i$ is 484, 230, −28, 290, and 290×10^{-3} GPa^{-1} for $i=1-5$, respectively. This indicates that phonon modes with 1000 cm^{-1} give the largest contribution to the thermal expansion in MoO_3, which is nearly two times that of those with 820, 250, and 100 cm^{-1}.

A linear Grünneisen constant can be obtained from the values of $n_i\kappa_{0x}\gamma_{ix}$ and n_i, as well as the reported values of the linear compressibility κ_{0x}. From the high-pressure studies of MoO_3 (Ref. 24), Åsbrink *et al.* confirmed that the compressibility in the *a* axis, normal to the stacking layers, shows a nonlinear behavior, and that in the *b* axis, the direction of O1—Mo—O1 chains, is very small. The values of the mean linear compressibility are reported to be $\kappa_{0a}=3.5\times10^{-2}$ GPa^{-1} over the low pressure range from 0 to 0.49 GPa, 1.1×10^{-2} GPa^{-1} over the high pressure range 1.54–7.41 GPa, $\kappa_{0b}=3.35\times10^{-4}$ GPa^{-1}, and $\kappa_{0c}=3.2\times10^{-3}$ GPa^{-1} over the whole pressure range 0–7.41 GPa. The bulk compressibility is $\kappa_0=3.86\times10^{-2}$ GPa^{-1} at low pressure and 1.46×10^{-2} GPa^{-1} at high pressure. Using the low-pressure values, the linear Grünneisen constant for the stretching frequency is evaluated to be $\gamma_{1a}=3.4$, $\gamma_{3b}=-20$, $\gamma_{2c}=18$ along the *a*, *b*, and *c* axes, respectively. The values for $i=4$ and 5 are $\gamma_{ia}=0.44$, $\gamma_{ib}=-2.2$, and $\gamma_{ic}=0.38$, which are one order of magnitude smaller than those of the stretching modes. Bulk parameter γ_i is 3.1, 1.5, −0.18, 0.42, and 0.42 for $i=1-5$, respectively (see Table IV). This indicates that 1000 cm^{-1} mode shows the largest pressure variation in phonon frequency, and 670 cm^{-1} one very slightly change. From the obtained values and the relation $\kappa_0\gamma_s=-(\partial\ln\omega_s/\partial p)$, we can predict that the frequency variation per 1 GPa must be 120, 47, and −4.7 cm^{-1} for 1000, 820, and 670 cm^{-1}, respectively. Thus, the remarkably large absolute values of the linear Grünneisen constant in the

TABLE IV. Calculated values of $x(0)$ and $V(0)$ including the zero-point vibrations, and evaluated linear and bulk Grünneisen constants, γ_{ix} and γ_i, using the reported values of linear and bulk compressibility, κ_{0x} and κ_0 (in units of 10^{-3} GPa^{-1}).[24] See the text for more details.

	Axis	a	b	c	Bulk
	$x(0)$ (Å)	13.744(4)	3.699(1)	3.957(1)	201.17(9) Å^3
	κ_{0x}, κ_0	35	0.335	3.2	38.6
i	n_i	γ_{ia}	γ_{ib}	γ_{ic}	γ_i
1	4	3.4(2)	0	0	3.1(2)
2	4	0	0	18(1)	1.5(1)
3	4	0	−20(2)	0	−0.18(2)
4	18	0.44(2)	−2.2(2)	0.38(4)	0.42(2)
5	18	0.44(2)	−2.2(2)	0.38(4)	0.42(2)

2D bonding network ($\gamma_{3b}=-20$, $\gamma_{2c}=18$) are proper to the strongly anisotropic MoO_3 crystals, but the pressure variation in the phonon frequencies of 670 and 820 cm^{-1} are very small due to the extremely small values of the linear compressibility in the network. Raman and infrared spectroscopic studies under high pressure will be needed to confirm this prediction. In order to make an analysis taking account of many low frequency phonons, which are oversimplified in the present study, very accurate and exact thermal expansion experiments down to low temperatures will be required.

Finally, we shall discuss these results from the ionic state of each atom and nature of the Mo—O bond. The ionic state of each atom is +3.0, −1.6, −0.7, and −0.8 for Mo, O1, O2, and O3 atoms, respectively, as mentioned already.[10] The bonds for Mo—O3 and Mo—O2a are very strong, where the minimum EDs for the Mo—O3 and Mo—O2a bonds are very high (1.99 and 1.78 eÅ^{-3}, respectively). The O1—Mo—O1 chain is arranged compactly with the minimum ED of 0.79 eÅ^{-3} for the Mo—O1a and Mo—O1c bonds. On the other hand, the van der Waals force between O3---O3 atoms along the a axis is weak and the van der Waals radius for the O3 atom can be estimated at about 1.42 Å, half of the distance between O3---O3 atoms at 300 K. Thus, O3 is a unique atom having both a strong covalent bond with the Mo atom and weak van der Waals bond with other O3 atoms, as shown in Fig. 6(a), where a schematic projection of the MoO_3 structure on the ab plane is depicted to emphasize the van der Waals radius for O3 atoms. With increasing temperature, the vibration of the Mo—O3 bond increases, and the effective van der Waals gap between the O3 atoms is expanded, which induces a remarkable increase in the lattice parameter a. Thus, the large thermal expansion of MoO_3 along the a axis is the resultant from the combination of the high frequency phonon vibration (1000 cm^{-1}) due to the strong Mo—O3 bond and the large compressibility of the van der Waals gaps between the O3---O3 atoms [Fig. 6(b)]. Such a result may be realized commonly in the layered materials which have some strong bonds along the stacking direction, but it may be not valid in those having rather weak bonds, such as transition-metal dichalcogenides, with a stretching phonon mode frequency lower than 350 cm^{-1}.[25] Their thermal expansion coefficients may saturate and be constant above 400 K within the quasiharmonic approximation. Furthermore, if the expansion along the a axis in MoO_3 is suppressed by applying a pressure, then a pressure-induced phase transition may occur in MoO_3 to relax some large thermal vibrational motion of the O3 atoms. In fact, the monoclinic high-pressure phase of MoO_3, the so-called MoO_3-II phase, has been synthesized under 973 K and 6 GPa, and its structural study at room temperature has confirmed that the individual layers themselves remain virtually unchanged, but the stacking sequence of the layers varies.[26] A high pressure study at high temperature using a diamond anvil cell is required to observe *in situ* the conversion to the monoclinic phase. First principles calculations of the crystal structure and electronic structure at zero and high pressure for various layered materials will give us more quantitative information beyond the quasiharmonic approximation, as done for diamond.[27]

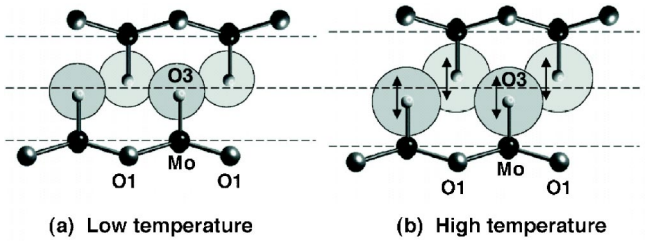

FIG. 6. Schematic projections of the structure of MoO_3 on the ab plane using an effective van der Waals radius for O3 atoms at (a) low temperature and (b) high temperature. The shaded circle centered at the O3 atom indicates the effective van der Waals radius, which expands with increasing temperature by the stretching phonon mode.

IV. CONCLUSION

We have found that two-dimensional insulator MoO_3 exhibits an anisotropic thermal expansion from 110 to 1000 K. MoO_3 expands remarkably along the a axis of the stacking direction of the layered sheets but remains almost unchanged in plane. The temperature variation in the thermal expansion of MoO_3 can be understood quantitatively based on the phonon modes, considering three stretching frequencies of the Mo—O bonds and two low frequencies. These results indicate the important role of the high compressibility due to the

van der Waals gap in the thermal expansion in MoO_3, together with high vibrational frequencies due to the strong Mo—O bonds. When employing MoO_3 as various devices or catalytic materials above room temperature, we obtain an advantage to control their characteristics with temperature through the anisotropic thermal expansion. Moreover, MoO_3 can be a candidate for insulating substrates or thin films requiring a small expansion of less than 1% in a two-dimensional plane below 1000 K.

ACKNOWLEDGMENTS

The authors thank Dr. E. Nishibori, Professor M. Takata, and Professor M. Sakata for their help in the Rietveld analysis, and H. Akamine for his experimental assistance. The experiments were performed at BL02B2 in SPring-8 with the approval of the Japan Synchrotron Radiation Research Institute (JASRI) (Proposal Nos. 2000A0131 and 2001B0457). The authors also thank Professor K. Kisoda for valuable and useful discussion about the phonon modes in MoO_3.

*Corresponding author. Email address: hnegishi@hiroshima-u.ac.jp

[1] L. J. Deiner, S. L. Wilcke, C. M. Friend, and F. C. Nart, Surf. Sci. **477**, L301 (2001).
[2] M. Itoh, K. Hayakawa, and S. Oishi, J. Phys.: Condens. Matter **13**, 6853 (2001).
[3] J. N. Yao, K. Hashimoto, and A. Fujishima, Nature (London) **355**, 624 (1992).
[4] C. M. Julien, Mater. Sci. Eng., R. **40**, 47 (2002).
[5] M. Greenblatt, Chem. Rev. (Washington, D.C.) **88**, 31 (1988).
[6] C. Schlenker, *Properties of Molybdenum Bronzes and Oxides* (Kluwer, Dordrecht, 1989).
[7] E. Canadell and M. H. Whangbo, Chem. Rev. (Washington, D.C.) **91**, 965 (1991).
[8] X. L. Li, J. F. Liu, and Y. D. Li, Appl. Phys. Lett. **81**, 4832 (2002).
[9] Y. Li and Y. Bando, Chem. Phys. Lett. **364**, 484 (2002).
[10] Y. Kuroiwa, N. Sato, A. Sawada, S. Negishi, H. Negishi, and S. Aoyagi, J. Phys. Soc. Jpn. **72**, 2811 (2003).
[11] L. Kihlborg, Arkiv Kemi **21**, 357 (1963).
[12] A. Papakondylis and P. Sautet, J. Phys. Chem. **100**, 10681 (1996).
[13] F. Zocchi, Solid State Sci. **2**, 383 (2000), and references therein.
[14] M. L. Tian, L. Chen, and Y. H. Zhang, Phys. Rev. B **62**, 1504 (2000).
[15] H. Negishi, Y. Kuroiwa, H. Akamine, S. Aoyagi, A. Sawada, T. Shoubu, S. Negishi, and M. Sasaki, Solid State Commun. **125**, 45 (2003).
[16] P. Kierkegaard, Arkiv Kemi **23**, 223 (1964).
[17] H. C. Zheng, J. Cryst. Growth **186**, 393 (1998); H. Negishi, T. Miyahara, and M. Inoue, *ibid.* **144**, 320 (1994).
[18] E. Nishibori, M. Takata, K. Kato, M. Sakata, Y. Kubota, S. Aoyagi, Y. Kuroiwa, M. Yamakata, and N. Ikeda, Nucl. Instrum. Methods Phys. Res. A **467-468**, 1045 (2001).
[19] Y. Kuroiwa, S. Aoyagi, A. Sawada, J. Harada, E. Nishibori, M. Takata, and M. Sakata, Phys. Rev. Lett. **87**, 217601 (2001).
[20] P. Brüesh, *Phonons: Theory and Experiments I* (Springer-Verlag, Berlin, 1982).
[21] M. A. Py and K. Maschke, Physica **105B**, 370 (1981).
[22] L. Seguin, M. Figlarz, R. Cavagnat, and J.-C. Lassegues, Spectrochim. Acta, Part A **51**, 1323 (1995), and references therein.
[23] M. Dieterle, G. Weinberg, and G. Mestl, Phys. Chem. Chem. Phys. **4**, 812 (2002).
[24] S. Åsbrink, L. Kihlborg, and M. Malinkowski, J. Appl. Crystallogr. **21**, 960 (1988).
[25] E. M. McCarron III and J. C. Calabrese, J. Solid State Chem. **91**, 121 (1991).
[26] B. L. Evans, in *Optical and Electrical Properties*, edited by P. A. Lee (Reidel, Dordrecht, 1976), p. 1.
[27] J. J. Xie, S. P. Chen, J. S. Tse, S. Gironcoli, and S. Baroni, Phys. Rev. B **60**, 9444 (1999).